SCIENCE CHINA
Information Sciences

Supplement for "Variational quantum eigensolver with linear depth problem-inspired ansatz for solving portfolio optimization in finance"

Appendix A Theoretical Analysis

In this appendix, we provide theoretical insights to some extent for why the proposed ansatze are capable of preparing arbitrary Dicke states efficiently with fairly low complexity. In the main text we show that CC ansatz is inspired directly by the structure of the circuit (Figure 1 for preparing W state. That is to say, the case of $|D_1^n\rangle$ in Dicke states is prepared by extracting the information stored in column 2^{n-1} of unitary U_n. In the following, we take $|D_k^5\rangle$ as the warm-up example to generalize the intuition for preparing arbitrary Dicke states. This idea is also likely to provide insights into why matrix product states and multiple layers of hardware-efficient (HE) ansatz can efficiently approximate quantum states.

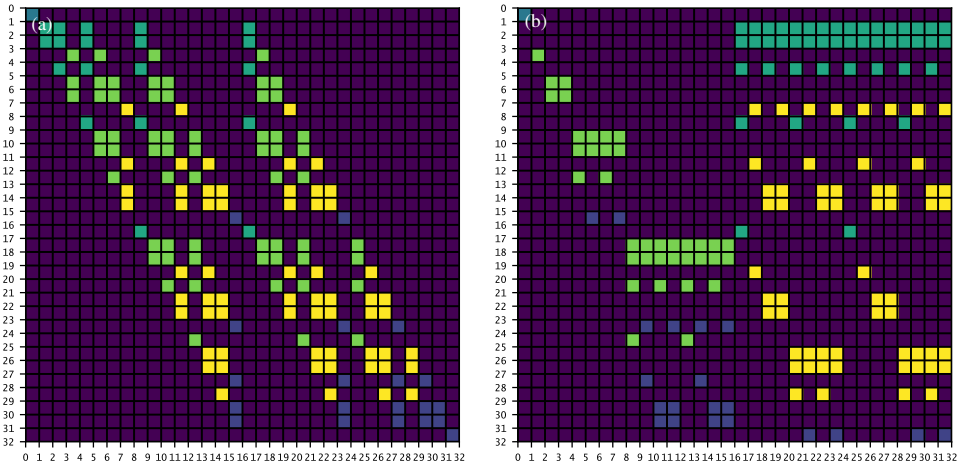

Figure A1 (Color online) The matrices for U_5 based on (a) 3C and (b) 2C blocks.

For CCC ansatz, the matrix of U_5 is shown in Figure A1(a), where zero elements are indicated by the purple squares, and non-zero elements are represented by other colored squares. As can be seen, the Hamming weight of the elements in each column is unique. Hence we can prepare arbitrary $|D_k^n\rangle$ precisely. Specifically, (I) the columns $8 = \mathbf{01}000_2$ and $16 = \mathbf{10}000_2$ indicated by cyan can both prepare $|D_1^5\rangle$. This is because the shift of the X gate between the highest and second highest qubits in the upper left region in Figure A2 only induces a bit flip for the following R_y rotation. (II) For the green case of $k = 2$, there are multiple choices that are the set of columns $9 = \mathbf{01}001_2, 12 = \mathbf{01}100_2$ or set of columns $17 = \mathbf{10}001_2, 20 = \mathbf{10}100_2$. For a quantum device with richer qubit connectivity beyond just linear-nearest-neighbour coupling, each set of columns could be prepared directly without introducing SWAP operations. Without loss of generality here we add $18 = \mathbf{10}010_2$ to the second set and form an exponential sequence composed of $1, 2, 4$ with the highest qubit fixed to be 1 to complete Figure A2. It can be found that the sequence of $1, 2, 4$ forms a $|D_1^3\rangle$ state. (III) The $k = 3$ case represented by yellow squares can be summarized in the same manner by inserting column $21 = \mathbf{10}101_2$ to the set composed of columns $19 = \mathbf{10}011_2$ and $22 = \mathbf{10}110_2$. The little difference is that the 3 low bits form a $|D_2^3\rangle$ state that is also a $k = 2$ case with $n = 3$ now. To sum up, for preparing target state $|D_k^n\rangle$, we need to prepare state $|D_{k-1}^{n-2}\rangle$ on the low $n-2$ bits and $|10\rangle$ on the highest 2 bits first; then for preparing intermediate state $|D_{k-1}^{n-2}\rangle$, we need to prepare $|D_{k-2}^{n-4}\rangle$ on the low $n-4$ bits and $|10\rangle$ on the highest 2 bits of the $(n-4)$ bits; ..., in a recursive way. The process can be formalized as

$$\begin{aligned} |D_k^n\rangle &= U_n|10\rangle|D_{k-1}^{n-2}\rangle, \\ |D_{k-1}^{n-2}\rangle &= U_{n-2}|10\rangle|D_{k-2}^{n-4}\rangle, \\ &\vdots \\ |D_{k-(i+1)}^{n-2(i+1)}\rangle &= U_{n-2(i+1)}|10\rangle|D_{k-i}^{n-2i}\rangle, \end{aligned} \tag{A1}$$

until one of the conditions $n - 2i = k - i$ and $k - i = 0$ is reached.

This circuit differs slightly from Figure 2(a) because the last 3C block in the dashed box (see Figure A2) is eliminated. Through a similar inspection, we establish the commonly constructive framework as presented in the main text. The reason for further eliminating the 3C blocks stems from the fact that multiple layers introduce additional symmetries that alter only the amplitudes, not the completeness, of the basis states. As analyzed above, we have diverse choices (different sets of equivalent columns) for constructing the same Dicke states with various circuit structures. Our hybrid distributed ansatze are determined in this manner, see section 4 and Appendix E.

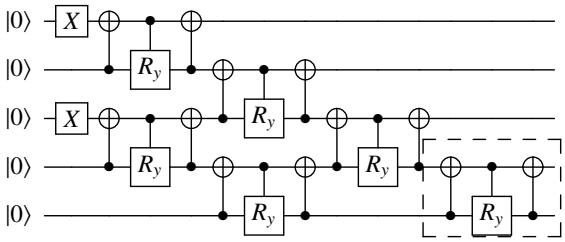

Figure A2 Illustration of the unsimplified version for preparing $|D_2^5\rangle$. The phase gates can be eliminated when 3C blocks are transpiled into the optimal circuits, see Appendix B for the optimal circuits.

The discussion of CC ansatz is in a similar way. The matrix of U_5 is shown in Figure A1(b). (I) As shown in the upper right of the figure, the cyan squares indicate the vectors with Hamming weight 1, i.e. the case of $k = 1$. There are 16 columns containing $\binom{5}{1}$, but just columns $16 = 2^4$ and 24 contain all of the five target vectors without redundancy. This corresponds to the case of preparing $|W_5\rangle$ state, see Figure 1. For the sake of uniformity and simplicity, column 16 has been chosen. (II) The row indices flagged by the green squares in the left side are the vectors with $k = 2$. The target basis states are dispersed in columns **1**, (**2**, 3), (**4**, 6), (**8**, 12) where the columns in the same parentheses contain the same target basis states. Obviously the exponential sequence composed of columns 1, 2, 4, 8 that is the $|W_4\rangle$ state perfectly constructs state $|D_2^5\rangle$, see Figure 2(b). That is to say, the linear combination required for extracting $|D_2^5\rangle$ is $|0\rangle|W_4\rangle$. (III) The yellow squares in the right side denote the $k = 3$ case where columns $17 = 16 + \mathbf{1}, 18 = 16 + \mathbf{2}, 20 = 16 + \mathbf{4}$ form the exponential sequence 1, 2, 4 by fixing the value of the highest qubit to 1. Similarly the exponential sequence 1, 2, 4 form the state $|W_3\rangle$ on the low 3 bits. The combined superposition state is $|10\rangle|W_3\rangle$ now. Therefore CC ansatz is constructed based on this generalized pattern, i.e. $|D_k^n\rangle = U_n S_k^n |0^n\rangle$ where S_k^n is the linear combination of columns for extracting $|D_k^n\rangle$ from U_n. S_k^n can be formalized for odd k as

$$\begin{aligned}
S_1^n &= NOT_1 \otimes I_{n-1},\\
S_3^n &= (I_2 \otimes U_{n-2})[(NOT_1 \otimes I_1) \otimes (NOT_1 \otimes I_{n-3})],\\
S_5^n &= (I_2 \otimes U_{n-4})(I_4 \otimes U_{n-4})[(NOT_1 \otimes I_1) \otimes (NOT_1 \otimes I_1) \otimes (NOT_1 \otimes I_{n-5})],\\
&\cdots\\
S_k^n &= [\prod_{i=0}^{\frac{k-3}{2}} (I_{(k-1)-2i} \otimes U_{n-(k-1)})]\{[\otimes_{i=0}^{\frac{k-3}{2}} (NOT_1 \otimes I_1)] \otimes (NOT_1 \otimes I_{n-k})\},
\end{aligned} \tag{A2}$$

and for even k as

$$\begin{aligned}
S_0^n &= I_n,\\
S_2^n &= (I_1 \otimes U_{n-1})(I_1 \otimes NOT_1 \otimes I_{n-2}),\\
S_4^n &= (I_1 \otimes U_{n-3})(I_3 \otimes U_{n-3})[I_1 \otimes NOT_1 \otimes I_1 \otimes NOT_1 \otimes I_{n-4}],\\
&\cdots\\
S_k^n &= [\prod_{i=0}^{\frac{k-2}{2}} (I_{(k-1)-2i} \otimes U_{n-(k-1)})]\{[\otimes_{i=0}^{\frac{k-2}{2}} (I_1 \otimes NOT_1)] \otimes I_{n-k}\}.
\end{aligned} \tag{A3}$$

However this state is not the exact $|D_k^n\rangle$ in the cases of $2 < k < n-2$ because a few extra basis states with Hamming weight not equalling k are introduced. For solving practical portfolio optimization with small k on NISQ computers, this is not the key problem. The strategies for mitigating this problem are presented in the main text and Appendix G. The critical is that CC ansatz has almost half the number of layers compared to CCC ansatz, which appears to be a beneficial characteristic. Furthermore, it provides us with a flexible way to regularly select the targets from a subspace that contains cases with multiple Hamming weights.

Appendix B Optimal Circuits for the Building Blocks

In the optimal two-qubit circuit theory [2], a two-qubit quantum gate $U \in \mathbf{SO}(4)$ can be constructed by 2 $CNOT$ gates and at most 12 elementary one-qubit gates in the magic basis

$$\mathcal{M} = \frac{1}{\sqrt{2}} \begin{pmatrix} 1 & 0 & i & 0 \\ 0 & i & 0 & -1 \\ 0 & i & 0 & 1 \\ 1 & 0 & -i & 0 \end{pmatrix},$$

with its circuit

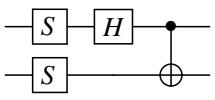

However, the optimal circuit for the 2C block contains 3 $CNOT$ gates because the 2C block belongs to $\mathbf{O}(4)$ with $\det(2C)= -1$ [2]. We set the determinant of 2C block to 1 by replacing the $CNOT$ gate with Controlled-$R_y(\pi)$.

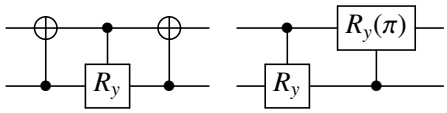

Figure B1 The building blocks of 3C (left) and 2C (right).

The two building blocks to be transformed are shown in Figure B1. Then based on $A \otimes B = \mathcal{M}U\mathcal{M}^\dagger$, 3C block and 2C block are mapped to $U_3(\theta/2,0,0) \otimes U_3(\theta/2,0,0)$ and $U_3(\theta/2,-\pi,\pi/2) \otimes U_3(\theta/2,-\pi,-\pi/2)$ respectively. Their elementary gate representations are $R_y(\theta/2) \otimes R_y(\theta/2)$ and $R_y^\dagger(\theta/2)S^\dagger \otimes R_y^\dagger(\theta/2)S$. Finally the optimal circuits are obtained based on $U = \mathcal{M}^\dagger(A \otimes B)\mathcal{M}$ as shown in Figures B2 and B3.

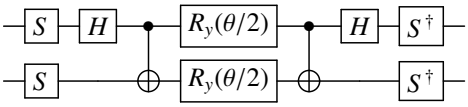

Figure B2 The optimal circuit for 3C building block with the parameter θ.

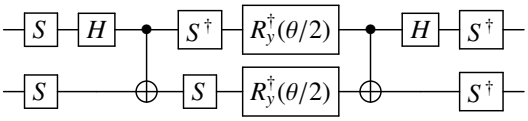

Figure B3 The optimal circuit for 2C building block with the parameter θ.

Another common method is the approximate compiling method that attempts to find the best approximate circuit V for the target U up to a global phase by minimizing the cost [3], e.g. the Frobenius norm $\frac{1}{2}||V-U||_F^2$. And the global phase introduces no impact to the evaluation of the Hamiltonian expectation, even in the circuit cutting scenario when all the elementary gates of each compiled V are partitioned into the same fragment. Therefore this strategy can be universally applied to both ansatze.

Appendix C Complexity Analysis of the Ansatze

In this appendix, we analyze the complexity of the CCC ansatz for preparing $|D_k^n\rangle$ with $k \leqslant \frac{n}{2}$. $|D_{n-k}^n\rangle$ can be prepared by $\otimes_{j=1}^n X_j|D_{n-k}^n\rangle$. Hence, the complexity of preparing $|D_{n-k}^n\rangle$ is equal to that of preparing $|D_k^n\rangle$. The number of 3C blocks (and parameters) used for constructing CCC ansatz accumulates as follows:

Layer	1	2	3	...	k
ith qubit	1	3	5	...	$2k-1$
# of 3Cs	$n-k$	$n-k-1$	$n-k-2$	...	$n-2k+1$

So the total number is the sum of the values in the arithmetic sequence above, calculated as $k(n-k)-\frac{k(0+k-1)}{2} = nk-\frac{3k^2}{2}+\frac{k}{2}$. Then when $k=\frac{n}{3}$, we can obtain roughly the highest complexity $\frac{n^2}{6}$.

The number of 2C blocks used for constructing CC ansatz can be evaluated as follows with odd k:

Layer	1	2	3	...	$\frac{k+1}{2}$
ith qubit	1	3	5	...	k
# of 2Cs	$n-1$	$n-3$	$n-5$	...	$n-k$

So the total number is about $(\frac{k+1}{2})(\frac{n-1+n-k}{2}) = \frac{n(k+1)}{2}-\frac{k^2}{4}-\frac{k}{2}-\frac{1}{4}$. The upper bound can be loosely set to $\frac{n^2}{4}$ when $k=\frac{n}{2}$. As can be seen, in the cases with large n and small k, the number of blocks used in CC ansatz is almost half that of CCC ansatz.

Appendix D Reduction of "Measure and Prepare" Channels

Reducing the sampling complexity is a major research direction for the practicality of circuit cutting technique [4, 5]. During the evolution of a quantum circuit, the invalid states will be automatically cancelled out based on the destructive inference phenomena. However, the circuit cutting technique distributes these redundant invalid components into different "measure-and-prepare" channels, which prevents the automatic cancellation. Specifically, a single qubit identity channel Id [1] can be decomposed as

$$\mathrm{Id}(\rho) = \sum_{i=1}^{8} c_i \mathrm{Tr}(O_i\rho)\rho_i, \tag{D1}$$

where the Pauli observables O_i, the corresponding eigenprojectors ρ_i, and the eigenvalues c_i are

$$\begin{aligned}
&O_1 = I, \quad \rho_1 = |0\rangle\langle 0|, \quad c_1 = +1/2,\\
&O_2 = I, \quad \rho_2 = |1\rangle\langle 1|, \quad c_2 = +1/2,\\
&O_3 = X, \quad \rho_3 = |+\rangle\langle +|, \quad c_3 = +1/2,\\
&O_4 = X, \quad \rho_4 = |-\rangle\langle -|, \quad c_4 = -1/2,\\
&O_5 = Y, \quad \rho_5 = |+i\rangle\langle +i|, \quad c_5 = +1/2,\\
&O_6 = Y, \quad \rho_6 = |-i\rangle\langle -i|, \quad c_6 = -1/2,\\
&O_7 = Z, \quad \rho_7 = |0\rangle\langle 0|, \quad c_7 = +1/2,\\
&O_8 = Z, \quad \rho_8 = |1\rangle\langle 1|, \quad c_8 = -1/2.
\end{aligned} \tag{D2}$$

As shown in Figure D1, a single qubit identity channel Id corresponds to a qubit segment without an operator acting on it, just like an identity operator I. Each single qubit identity channel Id is decomposed into 8 "measure-and-prepare" channels, preventing the automatic cancellation. In other words, the entanglement in the channel Id is decomposed into 8 subcircuits. Each subcircuit is a direct product of two fragments, and all fragments can be executed independently. Consequently, the circuit can be executed by a smaller quantum computer. However, this is also why the sampling complexity of the circuit cutting technique increases exponentially with the number of cut qubits. If the invalid states in different channels can be reduced in some way, the bulgy sampling complexity can slim down as well. Surprisingly, we found that, for CCC ansatze, all the redundancies can be eliminated when the number of cut qubit between the adjacent fragments is 1. The sampling complexity (number of subcircuits) reduces from $O(2^p)$ to $O(1)$, with p the total number of cut qubits.

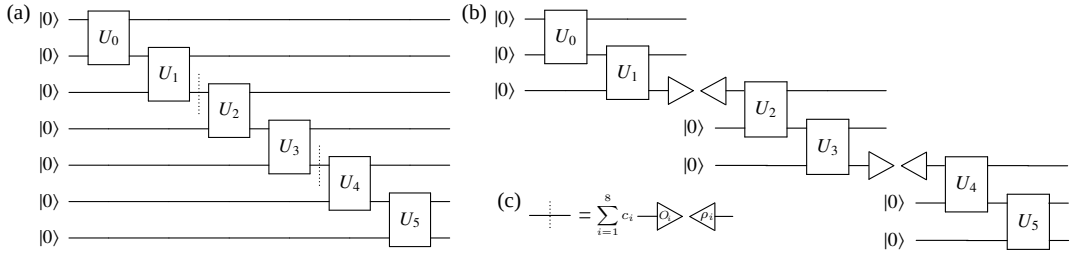

Figure D1 (a) An illustrative single-layer staircase structure circuit. Here, U_i is an arbitrary 2-qubit operator. The dotted lines denote the cut positions (qubits). (b) Each subcircuit is cut into 3 fragments. Each fragment can be executed independently using 3 qubits. A pair of triangles represents the "measure and prepare" channels between two adjacent fragments. (c) Each cut decomposes a single qubit identity channel Id into 8 "measure and prepare" channels. The total number of subcircuits is 8^2, and the total number of fragments is 3×8^2. It should be noted that each cut qubit is repeated in adjacent fragments. For instance, if the observables and eigenprojectors of both cut qubits are I and $|0\rangle\langle 0|$, and the outputs of the three fragments are $|10\mathbf{1}\rangle$, $|01\mathbf{1}\rangle$, and $|010\rangle$ (where the two bold "**1**" are the outputs of the two cut qubits), the output is recombined as $|1001010\rangle$.

Now, we assume that U_i is a 2-qubit 3C block and the NOT gates used to select specific columns are synthesized into U_i, as also illustrated in Figure D1. It's important to note that the amplitudes of the Dicke states prepared by our ansatze are real numbers. The first fragment, consisting of U_0 and U_1, also form a single-layer staircase structure circuit. Consequently, the state prepared by this fragment is a Dicke state with a unique k. (I) If the value of the cut qubit is 0, then the values of the uncut qubits are apparently different because they correspond to different basis states with the same Hamming weight k. (II) If the value of the cut qubit is 1, the uncut qubits are not equal to each other in the same way as when they have the unique Hamming weight $k-1$ now. (III) If the value of the cut qubit is a superposition of 0 and 1, then the uncut qubits are guaranteed to be different because basis states with different Hamming weights are different. Therefore, measuring the cut qubit in the X basis, see Figure D2(a), can be formalized as

$$\begin{aligned}
H \otimes I|\psi\rangle =& H \otimes I(|0\rangle \sum_x |\psi_x^0\rangle + |1\rangle \sum_y |\psi_y^1\rangle) = \frac{1}{\sqrt{2}}(|0\rangle + |1\rangle) \sum_x |\psi_x^0\rangle + \frac{1}{\sqrt{2}}(|0\rangle - |1\rangle) \sum_y |\psi_y^1\rangle\\
=& \frac{1}{\sqrt{2}}|0\rangle(\sum_x |\psi_x^0\rangle + \sum_y |\psi_y^1\rangle) + \frac{1}{\sqrt{2}}|1\rangle(\sum_x |\psi_x^0\rangle - \sum_y |\psi_y^1\rangle),
\end{aligned} \tag{D3}$$

where $\sum_x |\psi_x^0\rangle$ denotes the basis states with Hamming weight k, while $\sum_y |\psi_y^1\rangle$ denotes the ones with Hamming weight $k-1$. It is quite obvious that no interference happens among these states. So we have the reconstruction term [6]

$$\begin{aligned}
\mathrm{Tr}(\rho X) &= \mathrm{Tr}(\rho HZH) = \mathrm{Tr}(H\rho HZ) = \mathrm{Tr}(H\rho H(|0\rangle\langle 0| - |1\rangle\langle 1|))\\
&= \mathrm{Tr}(H\rho H|0\rangle\langle 0|) - \mathrm{Tr}(H\rho H|1\rangle\langle 1|) = \langle 0|H\rho H|0\rangle - \langle 1|H\rho H|1\rangle\\
&= p(|0\rangle|\psi'\rangle) - p(|1\rangle|\psi'\rangle) = 0,
\end{aligned} \tag{D4}$$

where $|\psi'\rangle$ is the state of uncut qubits. That is, the measurement in the X basis has no contribution to the reconstruction of useful information. A similar derivation for eliminating the Y basis, see Figure D2(b), is

$$(HS^\dagger) \otimes I|\psi\rangle = (HS^\dagger) \otimes I(|0\rangle \sum_x |\psi_x^0\rangle + |1\rangle \sum_y |\psi_y^1\rangle) = \frac{1}{\sqrt{2}}|0\rangle(\sum_x |\psi_x^0\rangle - i\sum_y |\psi_y^1\rangle) + \frac{1}{\sqrt{2}}|1\rangle(\sum_x |\psi_x^0\rangle + i\sum_y |\psi_y^1\rangle), \tag{D5}$$

the similar result can be obtained as $\mathrm{Tr}(\rho Y) = p(|0\rangle|\psi'\rangle) - p(|1\rangle|\psi'\rangle) = 0$.

In consequence, the preparations of $H|j\rangle\langle j|$ and $SH|j\rangle\langle j|$ at the corresponding channel of the second fragment, composed of U_2 and U_3, can be ignored, leaving $|0\rangle$ and $|1\rangle$ the only inputs. In this situation, the second fragment with input $|0\rangle$ or $|1\rangle$ is another Dicke state preparation circuit. In the iterative manner, the X and Y bases are eliminated in all fragments.

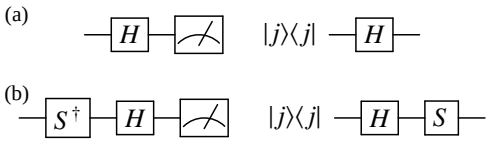

Figure D2 The decomposition of "measure-and-prepare" channels of (a) X basis, (b) Y basis. State $|j\rangle$ with $j \in \{0, 1\}$ is the measurement result.

Ultimately, the decomposition of the single qubit identity channel Id reduces to

$$\mathrm{Id}(\rho) = \sum_{i=1,2,7,8} c_i \mathrm{Tr}(O_i \rho) \rho_i. \tag{D6}$$

Further, the outputs of channels I and Z are the same, except the opposite sign in certain states. After cancelling these kind of states out, we found that the remaining states can be produced by observables $|0\rangle\langle 0|$ and $|1\rangle\langle 1|$ as

$$\rho = \langle 0|\rho|0\rangle|0\rangle\langle 0| + \langle 1|\rho|1\rangle|1\rangle\langle 1|. \tag{D7}$$

This can be regarded as the sub-channels of channel I, which only communicate useful information. The other sub-channels that communicate redundant information are eliminated. No redundancy means there is no need to perform extra sampling to eliminate the invalid states. As a result, the sampling complexity decreases to $O(\epsilon^{-2})$ with ϵ the accuracy. This is very amenable for circuit cutting-based distributed quantum computing because the sampling complexity no longer relates to the total number of cut qubits any more, which guarantees higher fidelity and lower variance of the result when cutting the original circuit into more fragments. This fits perfectly with our original idea of finding a larger-scale application suitable for the current NISQ computers. The result above inspires us that the identity channel Id should be able to be decomposable into fewer sub-channels when the state prepared by the ansatz possesses some form of symmetry or non-exponential degree of freedom.

However, the remaining observables $|0\rangle\langle 0|$ and $|1\rangle\langle 1|$ cannot be observed independently. Both states $|0\rangle$ and $|1\rangle$ should be measured in the I basis. Therefore, the fragments of each subcircuit should be sampled sequentially. Its procedure is as follows: (1) The first step is to measure the first fragment with the number of shots, say N, satisfying the sampling requirement, Hoeffding's inequality [1], on matrix basis I. The N measured strings are stored one by one according to the order in which they are measured and the number of the values 0 and 1 of the cut qubit are counted as N_0 and N_1, refer to Figure D1. The first fragment is submitted to the quantum computer once. (2) At the second step, the second fragment with input 0 and 1 are measured N_0 and N_1 times respectively. That is, two submissions of the second fragment were made, one with input 0 and the other with input 1. Based on the values of the cut qubit of the first N strings, the measured strings of the second fragment are appended to the first N strings one by one in accordance with their measured order. N_0 and N_1 are updated to be the number of the values 0 and 1 of the cut qubit of the second fragment. (3) Repeat step (2) until all fragments are appended. For instance, as illustrated in Figure E1(a), assume the measured strings of the first fragment are 01**0**, 00**1**, 10**0**, 00**1** with the last qubit being the cut qubit. Then the second fragment with inputs 0 and 1 are executed 2 times respectively. Assume the measured strings are 110_0, 011_0, and 111_1, 111_1 based on input 0 and 1 (represented as subscript) respectively, then the order corresponding to the first strings is 110_0, 111_1, 011_0, 111_1. So the combined basis states are 01110, 00111, 10011, and 00111. For a subcircuit with p cuts, the number of fragments submitted to the quantum computer is $2p + 1$. This is an exponential reduction compared to the circuit cutting technique.

CC ansatz is a little more complex because there are extra basis states that exist when k belongs to interval $[3, n-3]$. Fortunately we found that the Hamming weights of the extra basis states are all $k - 2i$ with positive integer i. This observation assures the validity of the conclusion for CCC ansatz, as the differences in the Hamming weights of their uncut qubits are at least 1. That is to say, the minimal difference between the nearest two Hamming weights of k and $k - 2$ is 1 when the values of the cut qubit are 1 and 0 respectively. In fact, the present result still holds when choosing multiple columns simultaneously, as the Hamming weights of the states prepared by this kind of subcircuits follow the above analysis.

Appendix E Experimental Schemes

For the cases of $k = 2, 3$ in CCC ansatz, the number of independent columns are $\lfloor \frac{n}{2} \rfloor$ and $\lfloor \frac{n-1}{2} \rfloor$ respectively. Here "independent" means any target basis state can only appear in a single column. In other words, there is no overlap between any two subspaces spanned by these subcircuits. For $k = 2$, we find that these are columns 3, 12, 48,..., $3 \times 4^{\lfloor \frac{n}{2} \rfloor - 1}$. Each column can be prepared by the column chosen circuit $X^{\otimes 2}$ operating on the corresponding qubits, e.g. column 3 corresponds to $X^{\otimes 2}$ operating on the lowest 2 qubits. For $k = 3$, these are columns $3 + 4^{\lceil \frac{n}{2} \rceil - 1}$, $12 + 4^{\lceil \frac{n}{2} \rceil - 1}$, $48 + 4^{\lceil \frac{n}{2} \rceil - 1}$,..., $3 \times 4^{\lfloor \frac{n-1}{2} \rfloor - 1} + 4^{\lceil \frac{n}{2} \rceil - 1}$. Each column can be prepared by $X^{\otimes 2}$ operating on the corresponding qubits and an X gate on qubit $2(\lceil \frac{n}{2} \rceil - 1)$ in the meantime, as depicted in Figure E1.

For CC ansatz, similar distribution pattern can be found. In $k = 2$ case, the ansatz is split into $\lfloor \frac{n}{2} \rfloor$ subcircuits, each of which corresponds to a pair of columns that are $(2^{n-3} \times 3, 2^{n-3} \times 1)$, $(2^{n-5} \times 3, 2^{n-5} \times 1)$, ..., and the last pair of columns is $(2^0 \times 3, 2^0 \times 1)$ when n is odd or the last column is 1 when n is even. Each pair of columns can be prepared by $R_y \otimes X$ operating on the corresponding qubits. The number of subcircuits is $\lfloor \frac{n-1}{2} \rfloor$ for the case of $k = 3$. The columns pair are $(2^{n-1} + 2^{n-4} \times 3, 2^{n-1} + 2^{n-4} \times 1)$, $(2^{n-1} + 2^{n-6} \times 3, 2^{n-1} + 2^{n-6} \times 1)$, ..., and the last pair of columns is $(2^{n-1} + 2^0 \times 3, 2^{n-1} + 2^0 \times 1)$ when n is even or the last column is 1 when n is odd. Each pair of columns can be prepared by $R_y \otimes X$ operating on the corresponding qubits and an X gate on the highest qubit in the meantime.

The above results can be verified easily via the matrix representation of U_n, see Figure A1 in Appendix A. When the ansatz is cut p times without classical splitting into subcircuits, the sampling complexities for $k = 2$ and $k = 3$ are $O(4^{2p})$ and $O(4^{3p})$ [7]

Table E1 Complexity of HDC scheme for cases of $k = 2, 3$ for both ansatze.

		# of subcircuits	# of Paras per sub
CCC ansatz	$k = 2$	$\lfloor \frac{n}{2} \rfloor$	$2i$, $i \in [\lfloor \frac{n}{2} \rfloor]$[1]
	$k = 3$	$\lfloor \frac{n-1}{2} \rfloor$	$n-1$
CC ansatz	$k = 2$	$\lfloor \frac{n}{2} \rfloor$	$2i$, $i \in [\lfloor \frac{n}{2} \rfloor]$
	$k = 3$	$\lfloor \frac{n-1}{2} \rfloor$	n

[1] $[\lfloor \frac{n}{2} \rfloor]$ refers to integers in interval $[1, \lfloor \frac{n}{2} \rfloor]$.

respectively. Commonly the total number of cut qubits p should be linear in n with the constant factor small enough to guarantee the advantage of quantum computing. Differently, here p has no impact on the sampling complexity $O(\epsilon^{-2})$ of each subcircuit explicitly. In the meantime, the errors can be mitigated more effectively by measurement error mitigation assisted by the symmetry property, see section 4 in the main text. In Table E1, we provide the detailed complexities of HDC for our ansatze with $k = 2$ and $k = 3$.

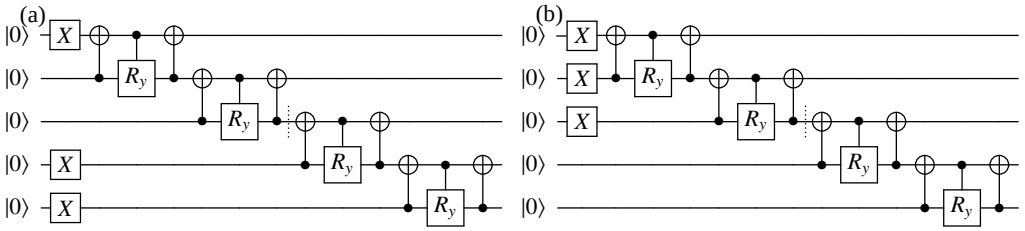

Figure E1 The two subcircuits for (a) column 19 and (b) column 28 of the CCC ansatz for preparing $|D_3^5\rangle$. The staircase U_n is straight. Each subcircuit is cut into 2 fragments. The dotted line denote the cut positions.

Without doubt, multiple columns can be prepared simultaneously to reduce the number of subcircuits. For more practical cases with much larger k, the number of independent columns increases in a superlinear manner in n. Hence we need to select multiple columns that overlap with each other, or import extra states, to obtain an affordable number of subcircuits that can provide quantum advantages, see Appendix A.

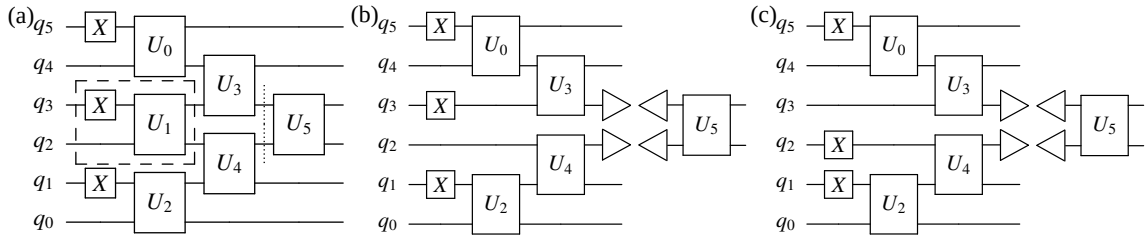

Figure E2 HDC design of $|D_3^6\rangle$. (a) The original CCC ansatz for preparing $|D_3^6\rangle$. The first step of HDC is to perform classical splitting of the circuit $U_1(X \otimes I)$ shown in the dashed box. The second step involves cutting the 2-qubit 3C block U_5 using circuit cutting technique. Circuit $U_1(X \otimes I)$ is decomposed into two product subcircuits, namely $X \otimes I$ and $I \otimes X$, while the other parts remain unchanged. (b) The first subcircuit. The staircase U_n is folded. $U_1(X \otimes I)$ is replaced by $X \otimes I$. Operator U_5 at the last time step is cut out to be simulated classically. The remaining two fragments are separable, which can be executed on a 3-qubit quantum computer. The upper fragment is a CCC ansatz for preparing $|D_2^3\rangle$, while the lower fragment is a CCC ansatz for preparing $|D_1^3\rangle$. (c) The second subcircuit. $U_1(X \otimes I)$ is replaced by $I \otimes X$.

In order to show the high scalability and flexibility of our HDC scheme for solving combinatorial optimization problems, here we provide a more practical scheme for partitioning the widely used Dicke state $|D_{n/2}^n\rangle$, which also reserves the identity channel Id of Equation (D7). In this situation, the straight staircase U_n (Figure E1) is replaced by the folded staircase U_n (Figure E2). We found that the CCC ansatz for preparing $|D_{n/2}^n\rangle$ can be classically split into $\frac{n}{2} - 1$ subcircuits, as illustrated in Figure E2. Each subcircuit is composed of two direct product $\frac{n}{2}$-qubit CCC ansatze, which are entangled by a 3C block at the last time step. These product CCC ansatze are $|D_{n/2-1}^{n/2}\rangle \otimes |D_1^{n/2}\rangle, |D_{n/2-2}^{n/2}\rangle \otimes |D_2^{n/2}\rangle, ..., |D_1^{n/2}\rangle \otimes |D_{n/2-1}^{n/2}\rangle$. Therefore, using the HDC scheme, the optimal solution can be searched within $\frac{n}{2} - 1$ subspaces. Each subspace is spanned by a subcircuit that can be simulated by a $\frac{n}{2}$-qubit quantum computer. For example, the Dicke state $|D_{30}^{60}\rangle$ can be classically split into 29 subcircuits, which has potential to achieve quantum advantage. The 29 subcircuits can then be executed using a 30-qubit quantum computer. In contrast, the most advanced circuit cutting technique [7] produces $O(4^{30})$ subcircuits to cut the CCC ansatz into two 30-qubit fragments. Our method achieves an exponential reduction.

Our numerical simulations show that, to obtain the optimal solution in the case $|D_{20}^{40}\rangle$, the classical brute-force takes over ten

days while the HDC scheme only takes several hours. The simulation of the 20-qubit fragments consumes most of the time. A personal computer with Intel(R) Core(TM) i5-10500 CPU @ 3.10GHz and 32GB RAM (2666MHz 16G × 2) is used.

To illustrate the effectiveness of the qubit reuse technique for executing the subcircuits produced by the HDC scheme, here we transfer the subcircuit shown in Figure E1(a) into the one shown in Figure E3. As can be seen in the figure, two qubits are sufficient to produce a basis state in column 19 of $|D_3^5\rangle$. Assume the qubits in Figure E1(a) are labeled as q_4, q_3, q_2, q_1, and q_0 from high to low. For the qubit reuse case shown in Figure E3, the measurements on the high qubit correspond to q_4, q_2, and q_0, while the measurements on the low qubit correspond to q_3 and q_1.

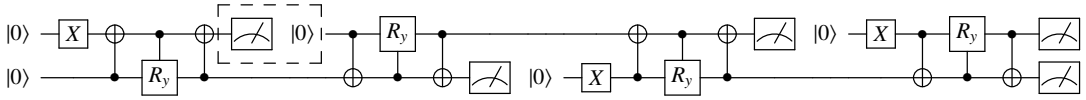

Figure E3 The subcircuit for column 19 of $|D_3^5\rangle$ in the qubit reuse form. The mid-circuit measurement and reset operations, illustrated in the dashed box, are the core of the qubit reuse technique.

Appendix F Experimental Setup

The configurations of the two experiments are shown in Table F1. The qubit performance and topology are provided in Table F2 and Figure F1, respectively. f_{00} (f_{11}) is the fidelity of measuring $|0\rangle$ ($|1\rangle$) when the true state is $|0\rangle$ ($|1\rangle$). As depicted in Table 1, the 2-qubit gate depth of CCC ansatze for preparing $|D_3^n\rangle$ and $|D_6^{12}\rangle$ is $2n-6$ and 12, respectively. However, the CCC ansatze for preparing $|D_3^n\rangle$ can be split into $\lfloor\frac{n-1}{2}\rfloor$ subcircuits with a single-layer staircase structure, see Table E1 and Figure E1. The 2-qubit gate depth of each subcircuit turns out to be $2(n-1)$, the same as $|D_1^n\rangle$. For each subcircuit, the number of 3-qubit fragments is $\lceil\frac{n-3}{3-1}\rceil+1=\lceil\frac{n-1}{2}\rceil$. This occurs because the cut qubit is repeated in adjacent fragments. Each 3-qubit fragment has a maximum 2-qubit gate depth of 4. For instance, as shown in Figure E1(a), when the cut qubit is prepared as $|0\rangle$, the 2-qubit gate depth of the second fragment is 2(3-1)=4. While when the cut qubit is prepared as $|1\rangle$, the 2-qubit gate depth is 0 (the two 3C blocks act as identity operators). According to the sequential sampling, see the second to last paragraph in Appendix D, the number of fragment submissions of each subcircuit is about $n-2$.

The CCC ansatz for preparing $|D_6^{12}\rangle$ is split into 5 subcircuits. Each subcircuit is cut into two 6-qubit fragments and one 2-qubit 3C block, as illustrated in Fgiure E2. Each 6-qubit fragment represents a CCC ansatz with a maximum depth of 10. Since the two 6-qubit fragments only involve the "measure" operation of the "measure and prepare" channel, they are each submitted to the quantum computer once. The 2-qubit 3C block is simulated classically, requiring no submission.

Table F1 Setup of simulations and experiments.

# of assets	5	15	25	35	45	55	12
IvCL[1]	0.2	0.1	0.05	0.05	0.025	0.025	0.0125
Shots in ICI [2]	8000	4000	2000	2000	1000	1000	3000
# of subcircuits	2	7	12	17	22	27	5
f/s[3]	2	7	12	17	22	27	2
fs/s[4]	3	13	23	33	43	53	2

[1] the Initial value of Confidence Level α.
[2] the Initial Confidence Interval $(0,\alpha]$.
[3] number of 3 (or 6)-qubit fragments per subcircuit.
[4] number of fragment submissions per subcircuit.

Table F2 Qubit performance.

Qubit	T_1(μs)	T_2(ns)	f_{00}(%)	f_{11}(%)	f_{SQ}(%)[1]	f_{CZ}(%)
Q45	26.6	354	97.3	93.1	99.75	97.31
Q46	23.8	707	95.1	92.4	99.61	97.11
Q52	19.3	977	97.0	92.6	99.81	98.16
Q53	31.4	629	97.2	94.1	99.82	98.00
Q54	22.7	5941	91.7	85.4	99.91	97.68
Q48	13.6	339	91.0	83.2	99.69	

[1] SQ represents single-qubit gate.

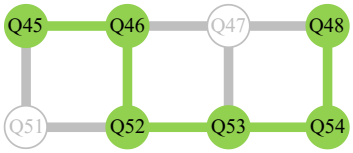

Figure F1 (Color online) The topology of the 6 used qubits.

Appendix G Symmetric Space Partition Scheme

According to the reverse symmetric property of Dicke state $|D_k^n\rangle$ mentioned in the main text, we can partition the space spanned by CC ansatz into two reverse symmetric subspaces, each of which contains one basis state of a symmetric pair that consists of two reverse symmetric basis states, such as 0011 and 1100, 1010 and 0101. Then we can employ one of the two subspaces as the search space, and perform the optimization process twice, corresponding to the assets in the original order and in the reversed order respectively. In practice, the perfectly bisected partition of these symmetric pairs is difficult to achieve. Hence we propose a compromised version that reduces non-targets to a large extent and preserves a reverse symmetric subspace, which is just required to remove the lowest $\lfloor\frac{n-k}{2}\rfloor+1$ 2C blocks in the staircase layer adjacent to U_n. This number has been confirmed through extensive numerical testing up to 29 qubits. In addition, a small number of basis states that are symmetrical, such as 10001, 01010, may not be contained in the search subspace which can be easily verified by directly calculating their expectations.

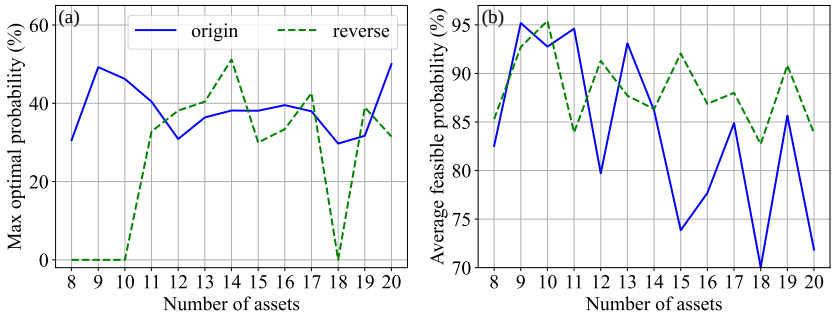

Figure G1 (Color online) The maximal/average probability of obtaining (a) the optimal solution and (b) the feasible solution up to 20 assets.

In this appendix, we also give the representative illustrations in Figure G1 of the symmetric space partition scheme. We performed a large number of numerical simulations and found that, in most of the experiments, both the subspaces spanned by the origin-order and reverse-order ansatze contain the optimal solution. Specifically to show the complementary characteristics of the two order cases in extreme cases, here the random seed 1213 for generating the financial data is chosen. The confidence level α is 0.25, and the budget is 4. And the simulation is performed with 5 different initializations of the parameters $\boldsymbol{\theta}$ in order to reduce the influence of bad parameter initialization, which could lead to the optimization converging to a result that contains the optimal solution with a tiny, even 0, probability. As illustrated in the figure, all pairs of ordered assets obtain the optimal solution with a sufficiently high probability. And the average probability of obtaining feasible solutions is always greater than 70%.

Appendix H Performance Comparison of Different Layers

Theoretically, a sufficient number of parameters enhances the expressibility of the ansatz which is beneficial for obtaining the optimal solution. However, in the NISQ era, more parameters seems not to be an efficient strategy. More parameters leads to an ansatz with more gates and depth, which induces more errors. The accumulation of these errors in the calculation of each expectation upon the corresponding parameter configuration during the optimization process introduces more serious instability, which hinders the selection of the optimization direction.

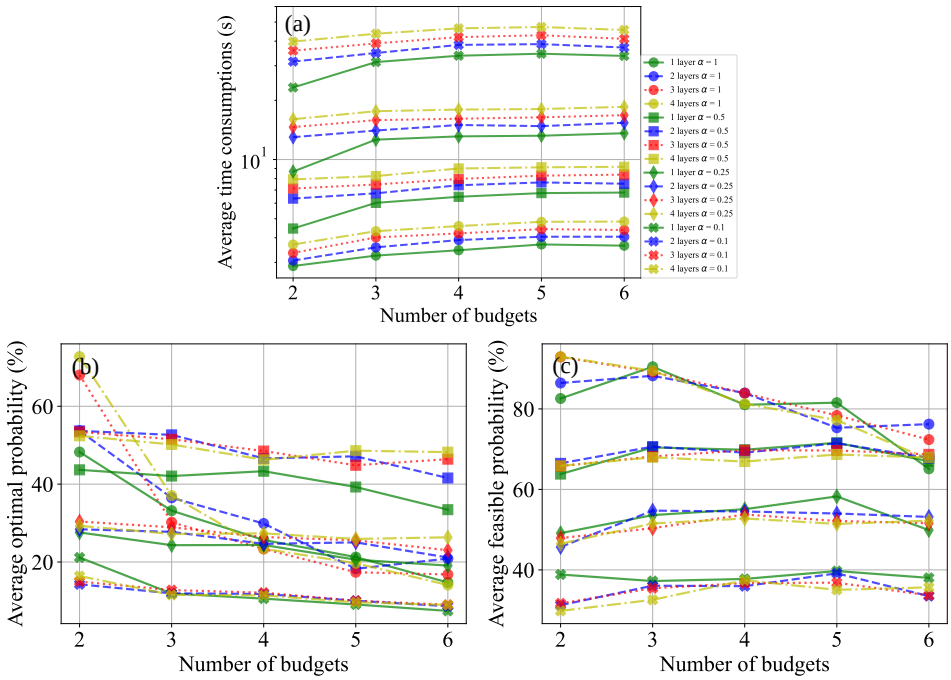

Figure H1 (Color online) Illustrative comparison of the performance of CCC ansatz with different layers of U_n upon different confidence levels.

The performance of CCC ansatz with 1 to 4 layers of U_n is illustrated in Figure H1. The number of assets is set to 12, and the asset pool is randomly initialized 50 times for each budget. The results indicate, on average, as the number of layers increases, the time consumption increases on the corresponding confidence level as expected. However the probabilities of obtaining the optimal and feasible solutions are almost the same for slightly smaller α. It is intuitive that the confidence level α should be reduced to the corresponding threshold for much bigger n and k. As can be seen, the CVaR cost function with a small enough confidence level

can guarantee the performance. Hence one layer of U_n with a small α seems to be a much better choice for solving combinatorial optimization problems, not only for the NISQ era.

References

1 Peng T, Harrow A W, Ozols M, et al. Simulating Large Quantum Circuits on a Small Quantum Computer. Phys Rev Lett, 2020, 125: 150504
2 Vatan F,Williams C. Optimal quantum circuits for general two-qubit gates. Phys Rev A, 2004, 69: 032315
3 Khatri S, LaRose R, Poremba A, et al. Quantum-assisted quantum compiling. Quantum, 2019, 3: 140
4 Perlin M A, Saleem Z H, Suchara M, et al. Quantum circuit cutting with maximum-likelihood tomography. npj Quantum Inf, 2021, 7: 64
5 Lowe A, Medvidović M, Hayes A, et al. Fast quantum circuit cutting with randomized measurements. Quantum, 2023, 7: 934
6 Tang W, Tomesh T, Suchara M, et al. CutQC: Using Small Quantum Computers for Large Quantum Circuit Evaluations. In: Proceedings of the 26th acm international conference on architectural support for programming languages and operating systems, 2021. 473–486
7 Harada H, Wada K, Yamamoto N. Doubly optimal parallel wire cutting without ancilla qubits. 2023. arXiv:2303.07340